

# Cloud regimes as phase transitions

Samuel N. Stechmann<sup>1,2</sup> and Scott Hottovy<sup>1</sup>

Submitted on December 15, 2015

Revised on April 29, 2016

Revised on May 23, 2016

## Key points

- Shallow cloud regimes fit the paradigm of a phase transition.
- This behavior can be seen in an idealized model of water as a stochastic diffusion process.
- Cloud area fraction can be highly variable at the interface of cloud regimes.

## Abstract

Clouds are repeatedly identified as a leading source of uncertainty in future climate predictions. Of particular importance are stratocumulus clouds, which can appear as either (i) closed cells that reflect solar radiation back to space or (ii) open cells that allow solar radiation to reach the Earth's surface. Here we show that these clouds regimes – open versus closed cells – fit the paradigm of a phase transition. In addition, this paradigm characterizes pockets of open cells (POCs) as the interface between the open- and closed-cell regimes, and it identifies shallow cumulus clouds as a regime of higher variability. This behavior can be understood using an idealized model for the dynamics of atmospheric water as a stochastic diffusion process. With this new conceptual viewpoint, ideas from statistical mechanics could potentially be used for understanding uncertainties related to clouds in the climate system and climate predictions.

## 1. Introduction

Clouds display a rich variety of forms. For example, intense rainfall is typically associated with deep clouds that fill the atmosphere up to cloud-top heights of roughly 10 km above the Earth's surface [Stevens, 2005]. On the other hand, shallow clouds have cloud-top heights of only 1–2 km above the Earth's surface, and while they are not associated with much rainfall, they have a major impact on climate [Ramanathan et al., 1989; Hartmann et al., 1992].

The climate impact of shallow clouds is largely due to their interactions with electromagnetic radiation. Clouds reflect solar radiation back to space, preventing the Earth from absorbing the radiation and thereby cooling the Earth. Furthermore, as can be seen from Fig. 1, some shallow clouds are more effective than others at reflecting solar radiation. The differences are nicely illustrated by the two

extreme types of stratocumulus clouds: closed-cell and open-cell [Agee et al., 1973; Wood, 2012]. Closed-cell stratocumulus clouds (Fig. 1a) cover essentially all of the underlying Earth's surface and can reflect a large portion of solar radiation. Open-cell stratocumulus clouds (Fig. 1c), on the other hand, have a broken cloud structure with open areas of clear skies at the center of cells with cloudy edges. Due to their smaller cloud fraction, open-cell stratocumulus clouds do not block much solar radiation and hence do not have a strong cooling effect on the Earth.

The net effect of shallow clouds on climate remains uncertain [Cess et al., 1990; Bony and Dufresne, 2005]. To better understand shallow clouds and their climate impact, several field campaigns have been carried out to gather and analyze observational data [Albrecht et al., 1995; Stevens et al., 2003; Bretherton et al., 2004; Rauber et al., 2007], and many detailed computer simulations have been performed and analyzed [Siebesma et al., 2003; Ackerman et al., 2004; Savijouvcic and Stevens, 2008]. The detailed computer simulations provide high-resolution information over limited geographic areas. Simulations of global climate, on the other hand, cannot represent shallow clouds in such detail, due to computational limitations. Instead, in global climate simulations, shallow clouds must be represented using simplified models [Cess et al., 1990; Bony and Dufresne, 2005]. Given the uncertainty of climate predictions, improved understanding is needed from simplified conceptual models.

One type of simplified model, long in use for studying the cloudy boundary layer, is the mixed-layer model [Lilly, 1968; Turton and Nicholls, 1987; Bretherton and Wyant, 1997]. For example, Bretherton and Wyant [1997] use a mixed-layer model to describe the transition between stratocumulus and shallow cumulus clouds. An even simpler type of model was presented by Chung and Teixeira [2012], where the cloud fraction is the only model output; i.e., no detailed information is included about the vertical or horizontal structure of the cloudy boundary layer. On the other hand, mixed-layer models describe the vertical structure of the cloudy boundary layer in some detail, while the horizontal structure is described only by horizontally averaged properties. In the present paper, in contrast, the vertical structure will be described only by vertically averaged properties, while horizontal variations are described in some detail using a stochastic model. An interesting future project is to combine these approaches to obtain a more realistic model of the cloudy boundary layer. In the present paper, however, the goal is to first investigate the horizontal variability in the simplest setting and to characterize cloud regimes based on horizontal structure.

In particular, here we will show that shallow cloud regimes fit the paradigm of a phase transition. More specifically, open-cell stratocumulus and closed-cell stratocumulus clouds correspond to two phases of cloud organization. The basis for the phase transition is partly from the accumulated knowledge from field campaigns, observational data analysis, and computer simulations [Albrecht et al., 1995; Siebesma et al., 2003; Stevens et al., 2003; Ackerman et al., 2004; Bretherton et al., 2004; Rauber et al., 2007; Savijouvcic and Stevens, 2008] and partly from a simplified model that we propose here to encapsulate these physical processes in idealized form.

<sup>1</sup>Department of Mathematics, University of Wisconsin–Madison, Madison, Wisconsin, USA.

<sup>2</sup>Department of Atmospheric and Oceanic Sciences, University of Wisconsin–Madison, Madison, Wisconsin, USA.

## 2. Idealized stochastic model of cloudy boundary layer dynamics

We propose here a simplified model for the dynamics of the cloudy boundary layer. The model is meant to be highly idealized and similar in complexity to models of phase transitions in other contexts, such as the Ising model for ferromagnetism [Yeomans, 1992]. As such, a single variable  $q(x, y, t)$  is used to represent the amount of total water (vapor plus liquid) in each column of the atmospheric boundary layer at horizontal spatial location  $(x, y)$ , minus a constant saturation value,  $q_{vs}$ . As a measure of integrated water, the units of  $q$  will be mm. The evolution in time is given by

$$\partial_t q = b\nabla^2 q - \frac{1}{\tau}q + D\dot{W} + F \quad (1)$$

where  $\nabla^2$  is the two-dimensional Laplacian,  $\partial_x^2 + \partial_y^2$ , and  $\dot{W}$  is spatiotemporal white noise. The four parameters  $b, \tau, D$ , and  $F$  are constants. The model in (1) can be related to atmospheric fluid dynamics, as described by Hottovy and Stechmann [2015a] and in the Supporting Information. In brief, the premise of the model is that boundary layer clouds can be understood in idealized form as resulting from the stochastic diffusion of total water.

The model in Eq. 1 was previously studied in the different context of deep convection in the tropics [Hottovy and Stechmann, 2015a], where it was shown to reproduce properties of self-organized criticality and the background power spectrum. In that case, the variable  $q$  represented the water in deep atmospheric columns, from the surface up to an altitude of  $O(10)$  km. Here, in contrast, the variable  $q$  represents only the water in the atmospheric boundary layer – i.e., in the lowest 1 or 2 km near the Earth’s surface. The main distinction between the two cases is in the parameter regimes: deep convection corresponds to a specific choice of parameter values, whereas shallow convection can take a richer variety of forms, as illustrated in Fig. 1, and is hence associated with a wide range of parameter values, as described further below.

The physical interpretations of the terms on the right-hand side of Eq. 1 are as follows, and they are illustrated schematically in the Supporting Information, Fig. S1. The first term,  $b\nabla^2 q$ , represents an eddy diffusion, which, as in common practice in fluid dynamics, is used to represent the mixing of the water due to the cumulative effects of many eddies. The second and third terms,  $-q/\tau$  and  $D\dot{W}$ , represent the simplest model for the turbulent fluctuations [Majda and Kramer, 1999; DelSole, 2004; Majda and Grote, 2007; Majda and Gershgorin, 2013], which are represented in idealized form as spatiotemporal white noise,  $\dot{W}$ , times the coefficient  $D$ , along with additional dissipation,  $-q/\tau$ , which allows a statistically stationary state to be achieved. In addition, the terms  $-q/\tau$  and  $D\dot{W}$  represent other physical processes with a random component, such as the entrainment into the cloud of unsaturated air from above the cloud (see Fig. S1), which is spatially and temporally variable due to turbulent eddies. Also note that the deterministic components of spatially varying surface evaporation and precipitation are often modeled with separate terms of the form  $-q/\tau_e$  and  $-q/\tau_p$  [Neelin and Zeng, 2000; Stevens, 2006], which have been merged together here and partially contribute to the single term  $-q/\tau$  in line with the goal of minimizing the number of model parameters. Finally, the last term,  $F$ , is a constant that represents a deterministic component of the net water sources and sinks; examples from Fig. S1 include precipitation and the evaporation of water from the ocean surface. In combination, the terms  $\tau^{-1}(q - \tau F)$  indicate that  $\bar{q} = \tau F$

is the mean value of  $q$ , which can be verified by taking the expected value of Eq. 1. In terms of  $q_t$ , since  $q = q_t - q_{vs}$ , the mean value is  $\bar{q}_t = q_{vs} + \tau F$ , which indicates that  $q_{vs}$  and  $\tau F$  enter the model in essentially the same way. In fact, one could alternatively use  $\bar{q}$  as the parameter instead of  $F$ ; however,  $F$  is used here in order to facilitate the analogy with ferromagnetism.

The relationship between the model parameters ( $D, F, b, \tau$ ) and environmental conditions (e.g., sea surface temperature (SST), lower tropospheric stability, etc.) is potentially complex, and how to specify such relationships is an issue for simplified models [Lilly, 1968; Turton and Nicholls, 1987; Bretherton and Wyant, 1997; Chung and Teixeira, 2012; Feingold and Koren, 2013; Ovchinnikov et al., 2013]. It would be interesting to examine these relationships in detail using observational or large eddy simulation data, and we plan a detailed investigation of this as future work. For the present investigation, however, we will work with some plausible relationships based on the great deal of insight provided by numerous previous studies [Bretherton and Wyant, 1997; Sandu et al., 2010; Sandu and Stevens, 2011; Chung and Teixeira, 2012].

As one example, to provide a physical context for thinking about different model parameter values, consider the SST. As described by the studies listed above and references therein, changes in SST have a significant impact on the properties of boundary layer clouds, as seen from a particular focus on the transition from stratocumulus to shallow cumulus clouds. More specifically, increases in SST cause an increase in surface latent heat flux (LHF), which could be interpreted as an increase in moisture source parameter  $F$  in the present model. However, this is not the totality of the effect of SST because with increased LHF comes higher turbulence levels (interpreted as higher values of parameter  $D$ ) and increased entrainment of warm, dry free-tropospheric air, whose drying effect could be interpreted as a decrease in parameter  $F$ . (The higher turbulence levels would probably also impact the other model parameters,  $b$  and  $\tau$ , although we will mainly discuss  $F$  and  $D$  here for simplicity.) This latter impact on  $F$  (a decrease) dominates over the former (an increase), and the stratocumulus layer thins and evaporates and gives way to shallow cumuli. Hence the net effect of increasing SST is a decrease in  $F$  and an increase in  $D$ .

For selecting values of the model parameters ( $b, \tau, D, F$ ), a method is used similar to Hottovy and Stechmann [2015a], except now applied to the case of shallow convection. Specifically, the model parameters  $b$  and  $\tau$  are related to the scales of spatial and temporal variability in the model [Hottovy and Stechmann, 2015a], and their values are chosen to be  $b = 25 \text{ km}^2 \text{ h}^{-1}$  and  $\tau = 100 \text{ h} \approx 4$  days to give a power spectrum consistent with observational data analyses of the variance of boundary-layer water vapor [Comstock et al., 2005], which roughly shows a “red” power spectrum, with largest variance on large scales and smaller variance on smaller scales. Furthermore, this value of  $\tau \approx 4$  days is also the same value estimated by Bretherton et al. [1995] for the dilution timescale due to entrainment. The value of  $D$  is related to the overall variance of total water, and the range of  $D$  values considered here is chosen to give variance values that are comparable to observational estimates of the variance of total water [Wood and Field, 2000; Larson et al., 2001] and liquid water path [Wood and Hartmann, 2006]. Finally, the parameter  $F$  represents the sum total of all mean sources and sinks of water, and the range of  $F$  values considered here is consistent with observational estimates of drizzle rates and latent heat fluxes, averaged over large scales, in the range of 0 to roughly 1 to 5 mm day<sup>-1</sup> [Bretherton et al., 1995, 2004; Comstock et al., 2007].

Also note that the potential spatial and/or temporal variations of the environmental conditions and hence model parameters are not considered in this first investigation, for

simplicity. Furthermore, the model parameters could themselves potentially be treated as interactive quantities that depend on the model variations in  $q(x, y, t)$ ; for example, radiative cooling should perhaps be an interactive quantity that depends on the cloud cover and hence on  $q(x, y, t)$ ; while perhaps more realistic, such a formulation comes at the expense of greater model complexity.

The saturation threshold is treated here as the fixed value  $q = 0$ , in accord with the definition of  $q$  as  $q = q_t - q_{vs}(T)$ , as described above Eq. 1. Quantities similar to  $q_t - q_{vs}(T)$  have also been used in previous studies [Mellor, 1977; Sommeria and Deardorff, 1977; Lewellen and Yoh, 1993], who describe their quantity as an extended liquid water specific humidity. Here, the total water,  $q_t$ , saturation water vapor,  $q_{vs}$ , and temperature,  $T$ , are interpreted as boundary-layer-column-averaged quantities, where  $q_{vs}(T)$  is a function of temperature given in terms of the Clausius–Clapeyron equation or perhaps a column-averaged version of it [Neelin *et al.*, 2009]. Also note that, due to the definition  $q = q_t - q_{vs}(T)$  and the temperature-dependence of  $q_{vs}$ , the sources and sinks of  $q$  could potentially arise from sources and sinks of heat. For example, the parameter  $F$  could potentially include the effects of radiative cooling, which decreases temperature  $T$  and in turn  $q_{vs}(T)$ , thereby acting as a source of  $q$  in this model. Finally, note that spatial variations in the saturation threshold are ignored here, for simplicity. A more realistic alternative is perhaps to model both the total water  $q_t(x, y, t)$  and the equivalent potential temperature  $\theta_e(x, y, t)$ , each of which could evolve according to a stochastic diffusion model such as (1), and from which one could determine spatially varying temperature  $T(x, y, t)$  and saturation water vapor  $q_{vs}(T(x, y, t))$ . While perhaps more realistic, such an approach also introduces additional complexity and model parameters; for this reason, we leave it as a future research direction, and we investigate only the simplest case here with only  $q$  and a uniform saturation threshold  $q = 0$ .

A cloud indicator variable  $\sigma(x, y, t)$  is defined based on whether or not  $q(x, y, t)$  is above the saturation threshold  $q = 0$  [Hottovy and Stechmann, 2015a]:

$$\sigma(x, y, t) = \begin{cases} 1 & \text{if } q(x, y, t) \geq 0, \\ 0 & \text{if } q(x, y, t) < 0. \end{cases} \quad (2)$$

Accordingly, if  $q \geq 0$ , then  $q$  is interpreted as liquid water, since  $q = q_t - q_{vs}$ . The transition from the absence of liquid water ( $q < 0$ ) to the presence of liquid water ( $q > 0$ ) is accompanied by a significant transition in albedo. Cloud albedo is also significantly affected by other factors such as in-cloud variability of liquid water content, which for simplicity is not indicated in the model results shown here but is a feature of the model.

For investigating Eq. 1, a discrete spatial grid is used with lattice spacing of  $\Delta x = \Delta y = 5$  km and square domain of side length  $L = 550$  km, and the stationary distribution of the stochastic model is sampled as described in the Supporting Information. This grid spacing is chosen partly to be comparable to the pixel width of the accompanying satellite images in Fig. 1, and partly to approximately correspond to the scale of convective elements in the boundary layer, which roughly scale with the boundary layer height of  $O(1)$  km, as indicated in Fig. S1. Numerical sensitivity studies with  $\Delta x = \Delta y = 1$  km show essentially the same results (see Supporting Information), and analytical results in the next section show a functional form of  $\sqrt{\log(L/\Delta x)}$ , which changes very slowly with changes in  $\Delta x$ , indicating robustness to changes in the grid spacing.

### 3. Cloud regimes as phase transitions

Examples of the model output are shown in Fig. 1e–h. The four cases represent the same four regimes of cloud or-

ganization shown in observational data in Fig. 1a–d, respectively. In addition to the cases of closed-cell and open-cell stratocumulus, the model also represents the case of pockets of open cells (POCs) [Stevens *et al.*, 2005], where closed and open cells can appear in comparable proportions. Finally, the fourth regime, shallow cumulus [Siebesma *et al.*, 2003; Rauber *et al.*, 2007], is shown in Figs. 1d and 1h and is characterized by small cloud elements and hence a small cloud area fraction. These four cloud regimes correspond to four distinct parameter regimes of Eq. 1, as described below.

To aid the interpretation of the model parameters, note that  $b$ ,  $D$ , and  $F$  are analogous to the three parameters of the well-known Ising model for ferromagnetism [Yeomans, 1992]: spatial interaction coefficient,  $J$ , temperature,  $T$ , and external magnetic field strength,  $H$ , respectively [Hottovy and Stechmann, 2015a]. The parameter  $\tau$  has no analog in the classic time-independent Ising model.

The proposed phase diagram of cloud regimes is shown in Fig. 2. In this diagram, the mean cloud area fraction,  $\bar{\sigma}$ , is shown for each choice of the parameters  $D$  and  $F$ . The value of  $\bar{\sigma}$  is defined as the expected value of  $\sigma(x, y, t)$ , in the stationary state, and it can be calculated analytically (see Supporting Information) as

$$\begin{aligned} \bar{\sigma} &= \frac{1}{2} \left[ 1 + \operatorname{erf} \left( \frac{\tau F}{\sqrt{2\operatorname{Var}(q_{ij})}} \right) \right] \\ &\approx \frac{1}{2} \left[ 1 + \operatorname{erf} \left( \frac{\tau F}{D} \sqrt{\frac{2\pi b}{\log(L/\Delta x)}} \right) \right], \end{aligned} \quad (3)$$

where  $\operatorname{Var}(q_{ij})$  is the variance of the water  $q(x, y, t)$  at lattice site  $(x, y) = (i, j)$ . Note that  $\operatorname{Var}(q_{ij})$  was previously presented by *Hottovy and Stechmann* [2015a], and here, in addition, we establish asymptotically that it depends on model parameters  $D$  and  $b$  as  $\operatorname{Var}(q_{ij}) \sim D^2(4\pi b)^{-1} \log(L/\Delta x)$  (see Supporting Information for derivation assuming  $\Delta x$  is small). Moreover,  $\bar{\sigma}$  depends on  $\sqrt{b}$  and  $\tau$  in the same way that it depends on  $F$ . For this reason, and in order to have a two-dimensional parameter space for plotting purposes, Fig. 1 shows  $\bar{\sigma}$  as a function of  $D$  and  $F$ , with  $b$  and  $\tau$  held fixed. This is analogous to typical presentations of the phase diagram of the Ising model, where it is common to fix the value of  $J$  and consider a range of values of  $T$  and  $H$  [Yeomans, 1992].

In Fig. 2, the closed-cell regime corresponds to  $F > 0$ , and the open-cell regime corresponds to  $F < 0$ . These two regimes correspond to cases of essentially full cloud cover and no cloud cover, respectively. In between the open- and closed-cell regimes, for  $F \approx 0$ , is a sharp transition in cloud area fraction, with POCs appearing in this sensitive parameter regime where cloud area fraction could take on intermediate values between 0 and 1. All of these stratocumulus cloud regimes are associated with relatively small  $D$  values and hence relatively low turbulent variability. For higher values of  $D$ , the water variability is higher, and clouds appear more intermittently, as in the case of shallow cumulus.

In addition to these traditional cloud regimes, many cloud scenes fall outside of this characterization and are somewhat disorganized [Wood and Hartmann, 2006; Wood, 2012]. For example, one such scene is displayed here in Fig. 1d, to the south and southwest of the yellow oval that indicates the shallow cumulus regime. In these southern parts of the panel, an appreciable amount of cloud cover is present, but it is not clearly organized as closed cells or open cells. In

Fig. 2, in the model, such cloud scenes are also present and are labeled as “unrobust phase.”

In nature, the cellular regimes and the unrobust regime are distinguished by the presence and lack of cellular structures, respectively. Here, in the simple model, such a distinction is not apparent, as the model does not represent the fine-scale details of the cellular nature of the open- and closed-cell regimes (see Fig. 1). Instead, here the cellular regimes and the unrobust regime are distinguished in another way: by their robustness and susceptibility, respectively, as described in the next section. It would be interesting to modify the model to allow a representation of the effects of individual cells [Koren and Feingold, 2011; Feingold and Koren, 2013; Ovchinnikov et al., 2013], which would prohibit the calculation of analytic formulas such as (3), but which would allow an investigation of the roles of both fine-scale and large-scale effects in determining cloud regimes. The appearance of cloud regime behavior from the model in (1) suggests that cloud regime behavior can possibly arise due to only large-scale factors – i.e., different environmental states ( $F$ ) and turbulent variability ( $D$ ) – and the presence of a saturation threshold.

#### 4. Susceptibility and climate uncertainty

In this section, the sensitivity, or susceptibility, of cloud fraction to changes in environmental parameters is investigated. The susceptibility will provide a second property, in addition to mean cloud fraction, that characterizes the different cloud regimes in the model. It is also a fundamental quantity of statistical mechanics [Yeomans, 1992; Christensen and Moloney, 2005; Majda et al., 2005], and, as such, it is a natural second quantity of interest in furthering the analogy between cloud regimes and traditional statistical mechanical phase transitions. Finally, since susceptibility is a measure of statistical sensitivity, it is a useful measure of climate response or climate uncertainty.

The susceptibility is defined as

$$\chi = \frac{\partial \bar{\sigma}}{\partial F} = \frac{\tau}{\sqrt{2\pi \text{Var}(q_{ij})}} \exp \left[ -\frac{(\tau F)^2}{2\text{Var}(q_{ij})} \right] \\ \approx \frac{\tau}{D} \sqrt{\frac{2b}{\log(L/\Delta x)}} \exp \left[ -\frac{2\pi b(\tau F)^2}{D^2 \log(L/\Delta x)} \right] \quad (4)$$

which follows from (3) as the derivative of mean cloud area fraction  $\bar{\sigma}$  with respect to the forcing  $F$ . This is analogous to the susceptibility that is commonly defined for magnetic systems [Yeomans, 1992].

A plot of the susceptibility  $\chi$  is shown in Fig. 2c. The most significant feature is the extremely high susceptibility of the POC regime: a small change in  $F$  leads to a very large change in cloud area fraction. On the other hand, the closed- and open-cell regimes have extremely low susceptibility and are instead robust to changes in  $F$ . Finally, we use the term “unrobust-phase” for the remaining cloud regimes where the susceptibility is moderate and in between these two extremes, corresponding with the disorganized cloud scenes seen in nature (e.g., in Fig. 1d, to the south and southwest of the yellow oval).

Based on these features of Fig. 2c, it is seen that the susceptibility  $\chi$  provides a second property, in addition to mean cloud fraction  $\bar{\sigma}$ , for the characterization of the model’s cloud regimes. More specifically, while the model does not resolve the details of the cellular structures that characterize the open- and closed-cell stratocumulus regimes in nature, it does represent the robustness of these clouds regimes in

terms of the low susceptibility of mean cloud fraction to changes in external forcing such as SST. In other words, the open- and closed-cell regimes are robust states in the sense that the mean cloud area fraction  $\bar{\sigma}$  in each case is essentially the same over a broad range of values of  $D$  and  $F$ ; on the other hand, shallow cumulus clouds and unrobust-phase or disorganized clouds have greater variability in the cloud area fraction. This model behavior here is an idealization, since, in nature, these properties are less clear-cut, and even a single cloud regime such as open-cell stratocumulus can exhibit different properties under different conditions; for instance, Martini et al. [2014] show that the depth of the boundary layer can influence the size of the cells which in turn influences the cloud albedo; and such effects of the details of individual cells are not currently included in the present results, in which the open-cell regime is idealized as a state with negligible cloud cover. Nevertheless, the present idealized model provides a simple basis to which additional physical processes could be included in the future.

The large susceptibility in some parts of Fig. 2c also indicates a potentially large source of inherent variability of the climate system. More specifically, if small changes occur in environmental factors such as sea surface temperature, then large changes can potentially arise in the mean cloud area fraction of shallow clouds, with consequences for the Earth’s radiative and energy budgets. Such large inherent variability can cause large uncertainty in projections of future climate. To fully understand the implications for climate uncertainty, however, the present model would need to be coupled with a more complete model of the climate system. An interesting future direction, in conjunction with a more complete climate model, is to use ideas from statistical mechanics such as the fluctuation–dissipation theorem [Leith, 1975; Majda et al., 2005] to better understand cloud statistics and implications for climate. Since the cloud indicator  $\sigma(x, y, t)$ , as defined in (2), is a nonlinear function of the underlying dynamical variables, it provides a challenging quantity to predict statistically [Gritsun et al., 2008]. It is interesting that, at least in the simplest setup used in the present paper, fluctuation–dissipation theory is not needed, and the susceptibility can be computed analytically as in Eq. 4.

While the present model is analogous to the Ising model in some ways, some notable differences can be seen in the behavior of the two models. For example, whereas the two-dimensional Ising model has a phase transition at a finite temperature [Yeomans, 1992], the present model appears to have a phase transition at  $D = 0$ , similar to the zero-temperature phase transition of the one-dimensional Ising model. Nevertheless, the large susceptibility near the critical point has important implications for climate applications in either case. It would be interesting to consider the effect of adding some nonlinear features [Stechmann and Neelin, 2011, 2014; Hottovy and Stechmann, 2015a, b] to Eq. 1 and to study their effect on the phase transition.

#### 5. Conclusions

In summary, shallow cloud regimes were shown to correspond with different phases of cloud organization, in a way that is conceptually analogous to the Ising-model representation of ferromagnetism [Yeomans, 1992]. In particular, open- and closed-cell stratocumulus clouds represent two opposing phases, POCs represent a type of critical phase at the interface of the open- and closed-cell phases, and shallow cumulus clouds represent a type of high-temperature phase with intermittent small-scale cloud elements. Accompanying this new conceptual viewpoint is the idea that the underlying physical processes can be understood in distilled form as the stochastic diffusion of water. In addition, this new conceptual viewpoint could potentially allow ideas from statistical mechanics to be used for understanding uncertainties related to clouds in the climate system and climate predictions.

**Acknowledgments.** The Moderate Resolution Imaging Spectroradiometer (MODIS) data from Fig. 1 is available from NASA at <https://ladsweb.nascom.nasa.gov/>.

The authors thank two anonymous reviewers for helpful comments that improved the paper. The research of S.N.S. is partially supported by a Sloan Research Fellowship, ONR Young Investigator Award N00014-12-1-0744, and ONR MURI grant N00014-12-1-0912. S.H. is supported as a postdoctoral researcher by the ONR grants. Computing resources were partially supported by ONR DURIP grant N00014-14-1-0251 and the University of Wisconsin-Madison Advanced Computing Initiative.

## References

- Ackerman, A. S., M. P. Kirkpatrick, D. E. Stevens, and O. B. Toon (2004), The impact of humidity above stratiform clouds on indirect aerosol climate forcing, *Nature*, *432*(7020), 1014–1017.
- Agee, E. M., T. S. Chen, and K. E. Dowell (1973), A review of mesoscale cellular convection, *Bull. Amer. Meteor. Soc.*, *54*(10), 1004–1012.
- Albrecht, B. A., C. S. Bretherton, D. Johnson, W. H. Scubert, and A. S. Frisch (1995), The Atlantic stratocumulus transition experiment—ASTEX, *Bull. Amer. Meteor. Soc.*, *76*(6), 889–904.
- Bony, S., and J. Dufresne (2005), Marine boundary layer clouds at the heart of tropical cloud feedback uncertainties in climate models, *Geophys. Res. Lett.*, *32*, 20,806.
- Bretherton, C. S., and M. C. Wyant (1997), Moisture transport, lower-tropospheric stability, and decoupling of cloud-topped boundary layers, *J. Atmos. Sci.*, *54*(1), 148–167.
- Bretherton, C. S., P. Austin, and S. T. Siems (1995), Cloudiness and marine boundary layer dynamics in the ASTEX Lagrangian experiments. Part II: Cloudiness, drizzle, surface fluxes, and entrainment, *J. Atmos. Sci.*, *52*(16), 2724–2735, doi:10.1175/1520-0469(1995)052<2724:CAMBLD>2.0.CO;2.
- Bretherton, C. S., T. Uttal, C. W. Fairall, S. E. Yuter, R. A. Weller, D. Baumgardner, K. Comstock, R. Wood, and G. B. Raga (2004), The EPIC 2001 stratocumulus study, *Bull. Amer. Meteor. Soc.*, *85*(7), 967–977.
- Cess, R. D., et al. (1990), Intercomparison and interpretation of climate feedback processes in 19 atmospheric general circulation models, *J. Geophys. Res.*, *95*(D10), 16,601–16,615, doi:10.1029/JD095iD10p16601.
- Christensen, K., and N. R. Moloney (2005), *Complexity and Criticality*, Imperial College Press, London.
- Chung, D., and J. Teixeira (2012), A simple model for stratocumulus to shallow cumulus cloud transitions, *J. Climate*, *25*(7), 2547–2554.
- Comstock, K. K., C. S. Bretherton, and S. E. Yuter (2005), Mesoscale variability and drizzle in southeast Pacific stratocumulus, *J. Atmos. Sci.*, *62*(10), 3792–3807.
- Comstock, K. K., S. E. Yuter, R. Wood, and C. S. Bretherton (2007), The three-dimensional structure and kinematics of drizzling stratocumulus, *Mon. Wea. Rev.*, *135*(11), 3767–3784, doi:10.1175/2007MWR1944.1.
- DelSole, T. (2004), Stochastic models of quasigeostrophic turbulence, *Surv. Geophys.*, *25*(2), 107–149, doi:10.1023/B:GEOP.0000028160.75549.0d.
- Feingold, G., and I. Koren (2013), A model of coupled oscillators applied to the aerosol–cloud–precipitation system, *Nonlin. Processes Geophys.*, *20*(6), 1011–1021, doi:10.5194/npg-20-1011-2013.
- Gritsun, A., G. Branstator, and A. Majda (2008), Climate response of linear and quadratic functionals using the fluctuation-dissipation theorem, *J. Atmos. Sci.*, *65*(9), 2824–2841, doi:10.1175/2007JAS2496.1.
- Hartmann, D. L., M. E. Ockert-Bell, and M. L. Michelsen (1992), The effect of cloud type on Earth’s energy balance: Global analysis, *J. Climate*, *5*(11), 1281–1304.
- Hottovy, S. A., and S. N. Stechmann (2015a), A spatiotemporal stochastic model for tropical precipitation and water vapor dynamics, *J. Atmos. Sci.*, *72*, 4721–4738, doi:10.1175/JAS-D-15-0119.1.
- Hottovy, S. A., and S. N. Stechmann (2015b), Threshold models for rainfall and convection: Deterministic versus stochastic triggers, *SIAM J. Appl. Math.*, *75*, 861–884, doi:10.1137/140980788.
- Koren, I., and G. Feingold (2011), Aerosol–cloud–precipitation system as a predator-prey problem, *Proc. Natl. Acad. Sci. USA*, *108*(30), 12,227–12,232, doi:10.1073/pnas.1101777108.
- Larson, V. E., R. Wood, P. R. Field, J.-C. Golaz, T. H. Vonder Haar, and W. R. Cotton (2001), Small-scale and mesoscale variability of scalars in cloudy boundary layers: One-dimensional probability density functions, *J. Atmos. Sci.*, *58*(14), 1978–1994, doi:10.1175/1520-0469(2001)058<1978:SSAMVO>2.0.CO;2.
- Leith, C. E. (1975), Climate response and fluctuation dissipation, *J. Atmos. Sci.*, *32*(10), 2022–2026, doi:10.1175/1520-0469(1975)032<2022:CRAFD>2.0.CO;2.
- Lewellen, W. S., and S. Yoh (1993), Binormal model of ensemble partial cloudiness, *J. Atmos. Sci.*, *50*(9), 1228–1237, doi:10.1175/1520-0469(1993)050<1228:BMOEPC>2.0.CO;2.
- Lilly, D. K. (1968), Models of cloud-topped mixed layers under a strong inversion, *Q. J. Roy. Meteor. Soc.*, *94*(401), 292–309.
- Majda, A. J., and B. Gershgorin (2013), Elementary models for turbulent diffusion with complex physical features: eddy diffusivity, spectrum and intermittency, *Phil. Trans. R. Soc. A*, *371*(1982), 20120,184, doi:10.1098/rsta.2012.0184.
- Majda, A. J., and M. J. Grote (2007), Explicit off-line criteria for stable accurate time filtering of strongly unstable spatially extended systems, *Proc. Natl. Acad. Sci. USA*, *104*, 1124–1129.
- Majda, A. J., and P. R. Kramer (1999), Simplified models for turbulent diffusion: theory, numerical modelling, and physical phenomena, *Phys. Rep.*, *314*(4), 237–574, doi:10.1016/S0370-1573(98)00083-0.
- Majda, A. J., R. V. Abramov, and M. J. Grote (2005), *Information Theory and Stochastics for Multiscale Nonlinear Systems*, CRM Monograph Series, vol. 25, 133 pp., American Mathematical Society, Providence.
- Martini, M. N., W. I. Gustafson, Q. Yang, and H. Xiao (2014), Impact of resolution on simulation of closed mesoscale cellular convection identified by dynamically guided watershed segmentation, *J. Geophys. Res. Atmos.*, *119*(22), doi:10.1002/2014JD021962.
- Mellor, G. L. (1977), The Gaussian cloud model relations, *J. Atmos. Sci.*, *34*(2), 356–358, doi:10.1175/1520-0469(1977)034<0356:TGCMR>2.0.CO;2.
- Neelin, J. D., and N. Zeng (2000), A quasi-equilibrium tropical circulation model—formulation, *J. Atmos. Sci.*, *57*, 1741–1766.
- Neelin, J. D., O. Peters, and K. Hales (2009), The transition to strong convection, *J. Atmos. Sci.*, *66*(8), 2367–2384.
- Ovchinnikov, M., R. C. Easter, and W. I. Gustafson (2013), Untangling dynamical and microphysical controls for the structure of stratocumulus, *Geophys. Res. Lett.*, *40*(16), 4432–4436, doi:10.1002/grl.50810.
- Ramanathan, V., R. D. Cess, E. F. Harrison, P. Minnis, B. R. Barkstrom, E. Ahmad, and D. Hartmann (1989), Cloud-radiative forcing and climate: Results from the Earth Radiation Budget Experiment, *Science*, *243*(4887), 57–63.
- Rauber, R. M., et al. (2007), Rain in shallow cumulus over the ocean: The RICO campaign, *Bull. Amer. Meteor. Soc.*, *88*(12), 1912–1928.
- Sandu, I., and B. Stevens (2011), On the factors modulating the stratocumulus to cumulus transitions, *J. Atmos. Sci.*, *68*(9), 1865–1881, doi:10.1175/2011JAS3614.1.
- Sandu, I., B. Stevens, and R. Pincus (2010), On the transitions in marine boundary layer cloudiness, *Atmos. Chem. Phys.*, *10*(5), 2377–2391, doi:10.5194/acp-10-2377-2010.
- Savic-Jovicic, V., and B. Stevens (2008), The structure and mesoscale organization of precipitating stratocumulus, *J. Atmos. Sci.*, *65*(5), 1587–1605.
- Siebesma, A., et al. (2003), A large eddy simulation intercomparison study of shallow cumulus convection, *J. Atmos. Sci.*, *60*(10), 1201–1219.
- Sommeria, G., and J. W. Deardorff (1977), Subgrid-scale condensation in models of nonprecipitating clouds, *J. Atmos. Sci.*, *34*, 344–355, doi:10.1175/1520-0469(1977)034<0344:SSCIMO>2.0.CO;2.

- Stechmann, S. N., and J. D. Neelin (2011), A stochastic model for the transition to strong convection, *J. Atmos. Sci.*, *68*, 2955–2970.
- Stechmann, S. N., and J. D. Neelin (2014), First-passage-time prototypes for precipitation statistics, *J. Atmos. Sci.*, *71*, 3269–3291.
- Stevens, B. (2005), Atmospheric moist convection, *Annu. Rev. Earth Planet. Sci.*, *33*(1), 605–643.
- Stevens, B. (2006), Bulk boundary-layer concepts for simplified models of tropical dynamics, *Theor. Comp. Fluid Dyn.*, *20*(5), 279–304.
- Stevens, B., et al. (2003), Dynamics and chemistry of marine stratocumulus – DYCOMS-II, *Bull. Amer. Meteor. Soc.*, *84*(5), 579–593.
- Stevens, B., G. Vali, K. Comstock, R. Wood, M. C. Van Zanten, P. H. Austin, C. S. Bretherton, and D. H. Lenschow (2005), Pockets of open cells and drizzle in marine stratocumulus, *Bull. Amer. Meteor. Soc.*, *86*(1), 51–57.
- Turton, J. D., and S. Nicholls (1987), A study of the diurnal variation of stratocumulus using a multiple mixed layer model, *Q. J. Roy. Meteor. Soc.*, *113*(477), 969–1009.
- Wood, R. (2012), Stratocumulus clouds, *Mon. Wea. Rev.*, *140*(8), 2373–2423, doi:10.1175/MWR-D-11-00121.1.
- Wood, R., and P. R. Field (2000), Relationships between total water, condensed water, and cloud fraction in stratiform clouds examined using aircraft data, *J. Atmos. Sci.*, *57*(12), 1888–1905, doi:10.1175/1520-0469(2000)057<1888:RBTWCW>2.0.CO;2.
- Wood, R., and D. L. Hartmann (2006), Spatial variability of liquid water path in marine low cloud: The importance of mesoscale cellular convection, *J. Climate*, *19*(9), 1748–1764.
- Yeomans, J. M. (1992), *Statistical mechanics of phase transitions*, Oxford University Press.

---

Corresponding author: S. N. Stechmann, Department of Mathematics, University of Wisconsin–Madison, 480 Lincoln Dr, Madison, WI 53706, USA. (stechmann@wisc.edu)

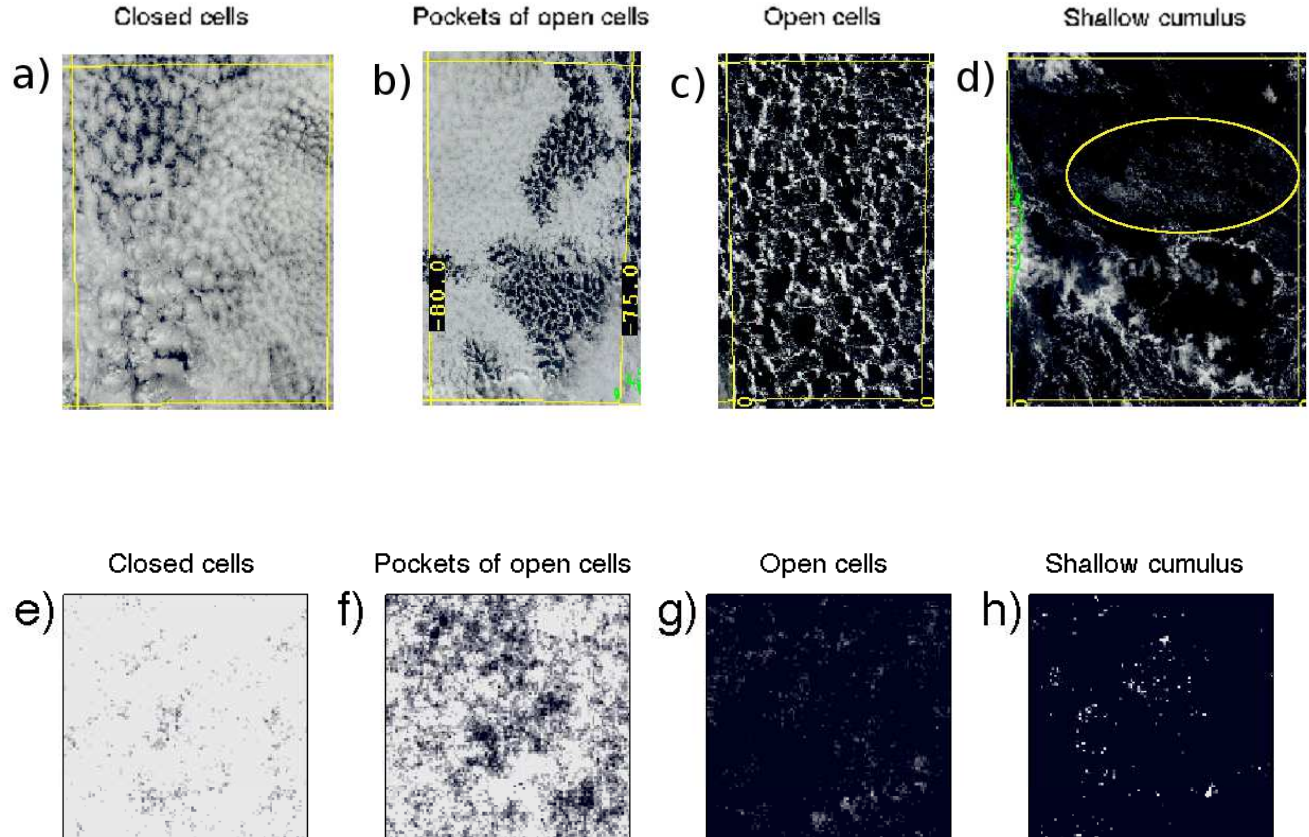


**Figure 1.** Four distinctive phases of shallow cloud organization, as viewed from satellite: (a) closed-cell stratocumulus, (b) pockets of open-cell stratocumulus, (c) open-cell stratocumulus, and (d) shallow cumulus (see interior of yellow oval). Yellow rectangles demarcate areas of  $5^\circ$  longitude by  $5^\circ$  latitude. Panels (e)–(h) show the same cloud regimes as in (a)–(d), respectively, except from the idealized model proposed here in Eq. 1. The model domain size is also  $5^\circ$  by  $5^\circ$ . The model cloud mask function is a smoothed version of the binary function  $\sigma(x, y)$ . See Supporting Information.

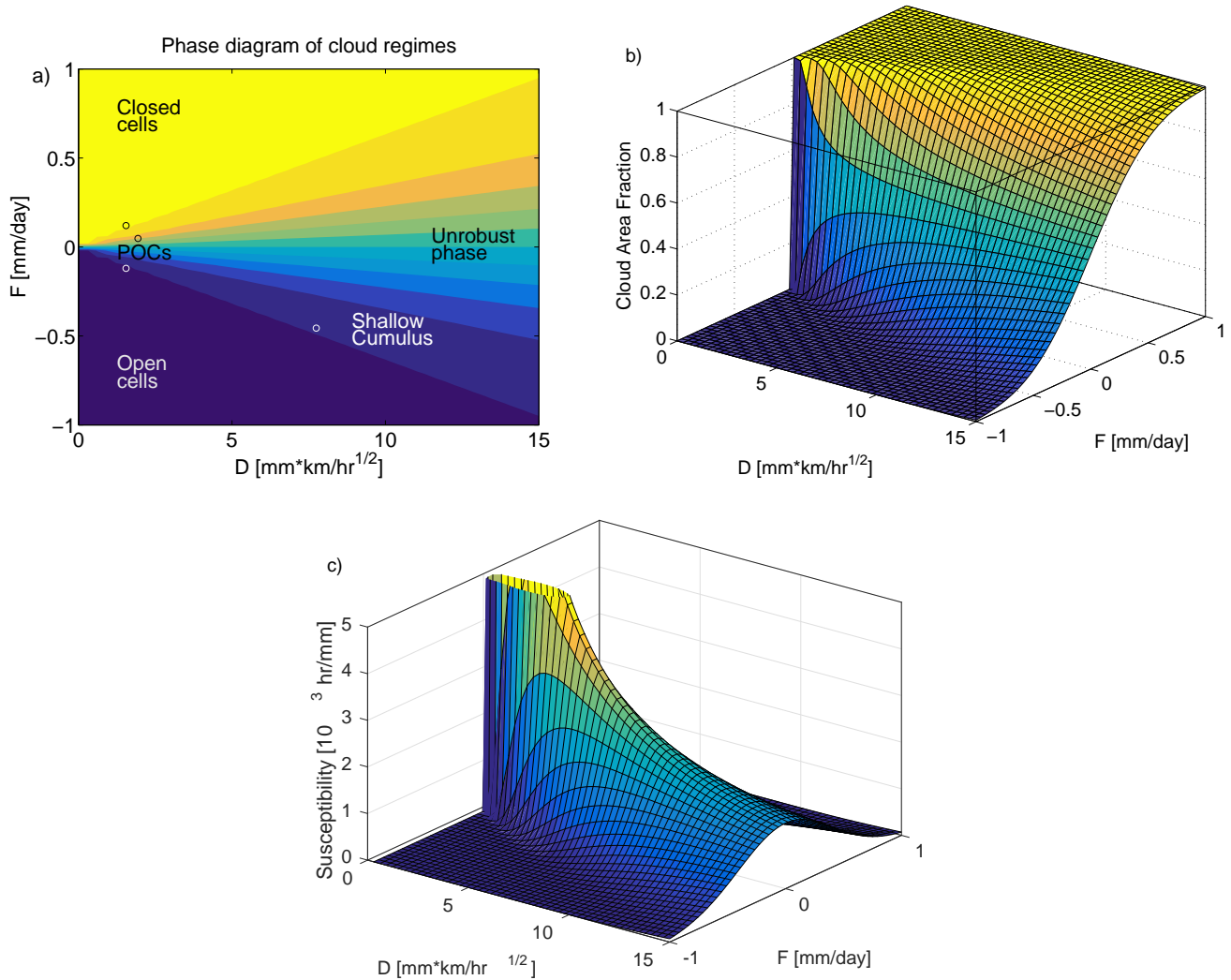


**Figure 2.** Phase diagram of shallow cloud regimes in the stochastic model from Eq. 1. (a) Contour plot of mean cloud area fraction,  $\bar{\sigma}$ , as a function of variability,  $D$ , and net source/sink,  $F$ . See Eq. 3. Four circles indicate the values of  $D$  and  $F$  used for Fig. 1e–h. (b) Same as (a), except a surface plot to highlight the phase transition. (c) Susceptibility,  $\chi$ , defined in Eq. 4 as  $\partial\bar{\sigma}/\partial F$ , shown as a function of  $D$  and  $F$ .